Tellus (2001), 53A, 481–499
Printed in UK. All rights reserved

TELLUS
ISSN 0280-6495

A numerical study of moist stratified flows over isolated topography

By M. M. MIGLIETTA[1]* and A. BUZZI[2], [1]*Institute for the study of Air Pollution and Agrometeorology, ISIAtA-CNR, Strada Provinciale Lecce-Monteroni, I-73100 Lecce, Italy and Italian Air Force Meteorological Service, Lecce Airport, I-73100 Lecce, Italy;* [2]*Institute of Atmospheric and Oceanic Science, ISAO-CNR, via Gobetti 101, I-40129 Bologna, Italy*

(Manuscript received 7 October 1999; in final form 13 November 2000)

ABSTRACT

In order to improve our understanding of orographic precipitation processes, a study of a 3-D flow over and around an isolated, Gaussian shaped mountain, with circular horizontal section, has been tackled. The effect of moisture is analysed systematically, by estimating the role of different parameters in the case of a simple stratified flow. The presence of humidity in the atmosphere can effectively change the flow regime with respect to the dry case, with the same wind and temperature upstream profiles. The energy exchange due to the release of latent heat tends, in general, to increase "flow over" an obstacle in detriment of "flow around". This result can be interpreted, to a first approximation, as a change in the local value of the Brunt–Väisäla frequency. However, as regards the interpretation of results, questions arise due to the irregular distribution of saturated portions, particularly downstream, and due to the fact that the volume of saturated air is a function itself of the flow regime near the obstacle. Some non-linear effects, such as the formation of upstream blocking and lee vortices, are confined to higher mountains in comparison with the dry case. The critical adimensional height for wave breaking is also moved by condensation to higher mountains, since moisture tends to decrease the wave amplitude. An increase of the adimensional height up to a certain value increases the volume of saturated air and the amount of precipitation; however, the opposite effect occurs for very high mountains. In general, the drag is strongly reduced in comparison with the dry case.

1. Introduction

The study of orographic moist flows concerns many different aspects of fluid dynamics in general, and of mesoscale meteorology in particular, such as orographic precipitation, drag, orographic waves, lee vortices. Previous studies on these subjects have considered mainly idealised 2-D topographies. Here we examine the problem of humid flow over an isolated, simply shaped 3-D mesoscale mountain, by adopting a numerical approach.

* Corresponding author.
e-mail: m.miglietta@isiata.le.cnr.it

The understanding of precipitation processes is fundamental in the effort of improving weather forecasts over mesoscale mountains. Laboratory experiments, numerical simulations at ever increasing resolution, and field experiments using advanced instruments, are used synergically in order to shed light on this important subject.

The local control of precipitation is one of the main ways the orography influences meteorological conditions. A number of different factors can influence the distribution and the intensity of orographic precipitation, such as large scale conditions, the shape and dimensions of the obstacle, the ground temperature, the vertical profile of wind, temperature and moisture. A very important dynamical role is played by latent heat release, that, in saturated ascending motion, changes the stability properties of a stratified atmosphere. In addition, cooling due to evaporation of precipitation and melting of falling snow can have important effects on flow properties in the presence of orography.

Although mountain waves have been widely studied, the role of humidity on wave dynamics has been generally neglected. Dry theories have been able to justify, at least in a partial and qualitative way, most of the observed phenomena. Nevertheless, the presence of large cloudy regions can change flow dynamics significantly (Cotton and Anthes, 1989): gravity waves depend on the stability of the atmosphere, that is strongly reduced if the atmosphere is saturated. Durran and Klemp (1982a) showed in 2-D numerical simulations that changes in the upstream moisture can strongly modify the structure of lee waves.

Moist equations are generally too complex to be solved with analytical methods, unless moist processes are approximated in very idealised conditions (Barcilon and Fitzjarrald, 1985; Barcilon et al., 1979; Fraser et al., 1973; Smith and Lin, 1982). Durran and Klemp (1982b) adopted linearised equations of motion, expressed in the same form in dry and saturated atmospheres: the effect of latent heat was included by simply solving dry equations where cloudy areas were replaced by dry regions of reduced stability. However, this equivalence is true only if N, the Brunt–Väisala frequency, is piecewise constant with height, that is not correct in the real atmosphere with deep clouds. The correct expression of the moist value of N has been calculated by considering the hypothesis that the atmosphere is saturated and by neglecting precipitation (Lalas and Einaudi, 1974; Durran and Klemp, 1982b).

As in inviscid dry simulations, the influence of orography on the flow depends mainly on two parameters: the adimensional height of the mountain (or the inverse Froude number) $H = h_{\max} N/U$, that is the maximum height $h_{\max}$ divided by the vertical gravity wave length ($2\pi U/N$, where U is a typical upstream wind speed), and a shape parameter $\beta = L_y/L_x$, the ratio between the transversal and the longitudinal characteristic width of the obstacle. Dry simulations with the same values of H and β should exhibit the same regime of flow. The presence of humidity introduces a new parameter; however, we will show that its effect can be interpreted, to some extent, as a change in the local value of Brunt–Väisala frequency N.

The energy contribution due to latent heat release can increase orographic "flow over" in detriment of "flow around". So, latent heat can modify the interaction between flows and mountains and produce interesting effects on the distribution and the intensity of orographic precipitation (Katzfey, 1995; Buzzi and Foschini, 1998; Buzzi et al., 1998a, b).

The most powerful and flexible approach to the full 3-D problem is numerical, since it allows the study of analytically unsolvable problems and a more complete description of moist processes. Only 2-D simulations of moist flows have been presented so far over idealised topography. Durran and Klemp (1982a) used a non-hydrostatic, compressible model to integrate numerically moist equations over a "witch of Agnesi" shaped mountain and over a realistic topography, simulating the downslope windstorm of January 1972 in Colorado. Wind field perturbations turn out to be weaker than in the dry case, and also the vertical profile of momentum flux is strongly reduced by humidity. Lilly and Durran (1983) included a simple parameterization of precipitation, that does not change in a significant way the previous moist results. Further 2-D simulations (Jusem and Barcilon, 1985) have stressed the effect of moisture on the reduction of drag and on the delay in formation of critical conditions that produce wave breaking.

The presence of moisture may have interesting effects on the drag in 3-D cases too, in particular in parameterizing the mountain drag in global models, where the orographic drag influences strongly the zonal circulation. As we will show, the moist dynamics can change the intensity of the drag dramatically, at least according to our idealised simulations.

2. Model characteristics and validation

The simulations presented here have been carried out using a channel version of the BOLAM3 model, that includes a simplified, explicit treatment of microphysical processes. BOLAM3 (BOlogna Limited Area Model), developed mainly at CNR-ISAO (Buzzi et al., 1994; Buzzi and Malguzzi, 1997; Buzzi and Foschini, 2000), is a meteorological mesoscale model: its dynamics is based on hydrostatic primitive equations. The dependent variables of these equations are wind components u and v, potential temperature θ, specific humidity q and surface pressure p_s, and 5 different hydrometeors. The horizontal discretization is based on an Arakawa C-grid. The vertical coordinate is σ and the choice of levels has been done in order to have a better resolution near the ground. The variables are distributed on a non-uniformly spaced staggered Lorenz grid. Second-order horizontal and vertical differencing is employed. A 2nd-order, forward-backward, three-dimensional advective scheme (Malguzzi and Tartaglione, 1999), stable up to Courant number equal 2, and a split-explicit time scheme, with forward-backward integration of gravity modes, have been implemented.

The flow is non-rotating and inviscid, in the sense that free-slip conditions are applied to the bottom. However, the presence of internal diffusion makes the flow not completely inviscid. A 4th-order horizontal diffusion term, based on a ∇^4 spatial operator, is added to all the prognostic equations, except for the tendency of surface pressure. A second-order divergence diffusion is included too, with a sponge layer (Klemp and Lilly, 1978) designed to damp the upward propagating wave energy before it is reflected from the upper surface. Therefore, the divergence damping is used with a modulated coefficient, which increases slowly with height, in order to minimise reflection that might occur as a consequence of rapid changes in its amplitude. The damping coefficient ν depends on the level k (increasing from top to bottom) in the following way:

$$\nu = 13\nu_0, \qquad 1 \leqslant k \leqslant 5, \tag{1}$$

$$\nu = 13\nu_0 \sinh\left(\frac{\pi}{2}\,\frac{\sigma(k) - \sigma\left(5 + \dfrac{\mathrm{NLEV}}{4}\right)}{\sigma(6) - \sigma\left(5 + \dfrac{\mathrm{NLEV}}{4}\right)}\right) \qquad 6 \leqslant k \leqslant 5 + \frac{\mathrm{NLEV}}{4}, \tag{2}$$

$$\nu = \nu_0 \qquad 5 + \frac{\mathrm{NLEV}}{4} \leqslant k \leqslant \mathrm{NLEV}. \tag{3}$$

The value of ν_0 is set to $0.8 \times 10^5\ \mathrm{s}^{-1}$; NLEV is the number of σ-levels, generally equal to 35. No additional dissipating factors are present in the model.

For the channel version, many different options of lateral boundary conditions have been employed: in our simulations, they are prescribed using a relaxation scheme (Davies, 1976; Lehmann, 1993) that absorbs internal wave reflection. Also for the inflow and outflow boundaries, an external border of 8 grid points is used to match the internal fields to the external constant values. Additional simulations have been carried out using reflecting lateral boundaries and periodic conditions at the entrance and at the end of the channel; however, solutions in the interior do not change significantly as a function of the boundary condition type.

Since many different parameters influence the solutions, we have decided to study flows with simplified physics: so, surface and boundary layer processes, radiation and convective parameterization are not active in our simulations. A dry adiabatic adjustment is, however, introduced in order to produce a gradual adjustment of potential temperature to a neutral profile in the case of superadiabatic profiles.

The water cycle is based on five explicit prognostic variables: cloud ice, cloud water, rain, snow and graupel. Since we are interested in moist and precipitation effects, such processes are dealt with in some detail. The most important microphysical processes are parameterized as a function of the local thermodynamic variables and the concentration of condensate, in a way similar, for several aspects, to the NEM scheme proposed by Schultz (1995). A semi-Lagrangian scheme for the 3-D advection and fall of the hydrometeors is implemented.

Initial conditions are defined through analytical relationships that calculate 3-D fields on the model grid, using pressure as vertical coordinate, before interpolating to sigma coordinates. Wind speed ($U = 10\ \mathrm{m\,s^{-1}}$, $V = 0$), dry Brunt–Väisäla frequency ($N = 1.34 \times 10^{-2}\ \mathrm{s}^{-1}$), surface temperature ($T_s = 20°\mathrm{C}$), surface pressure ($p_s = 1013$ hPa at $z = 0$) are prescribed as initial conditions and are kept fixed at the entrance of the channel during the experiments. Values are chosen in such a way that the atmosphere remains convectively stable, though close to neutrality, both upstream and over the obstacle, for most of the cases considered here, that is with upstream humidity $\leqslant 98\%$. This reflects observed conditions in some events of heavy orographic precipitation (Buzzi et al., 1998a, b).

In all the standard experiments (except for high-resolution preliminary tests — see below), we have used 35 σ-levels, while the horizontal distance between adjacent grid points carrying the same variable is 15 km. The number of grid points is 139 in the longitudinal direction and 73 in the latitudinal direction. The channel is wide enough to avoid that reflections from lateral boundaries may interfere with the solution near the obstacle. The value of the time step (120 s, with 30 s for the integration of gravity mode) assures stability and convergence to the numerical scheme.

The prescribed orography is Gaussian, with horizontal circular section:

$$h = h_{\max} \exp(-(x/L)^2 - (y/L)^2), \qquad (4)$$

and the characteristic length has been fixed to $L =$ 50 km. In the range of scales between 10 and 100 km, the flow properties are relatively insensitive to the mountain width (Smith, 1979). This mountain shape, although does not have the simple analytical properties of the bell-shaped mountain used by Smith (1980), has been studied before. With a Gaussian mountain, the action of non-linearity in modifying the prediction of linear theory is emphasised (Smith and Grønås, 1993). The mountain is introduced impulsively: the various techniques used in the literature to insert topography into models have no consequences on the results of simulations, after a reasonable time of integration. Palm (1953) showed that all transients decay as $O(t^{-1})$. Therefore, solutions are shown after all the transitional features have been advected far downstream. Residual non-stationary effects can be attributed to unstable features, such as downstream vortices or upstream propagating modes (Baines and Hoinka, 1985; Smolarkiewicz and Rotunno, 1990). In fact, non-stationarity is an intrinsic property of the flow for this range of parameters (Smolarkiewicz and Rotunno, 1990). High mountains and dry flows need a longer time to obtain quasi-stationary solutions.

Since the upstream values of U and N (dry) are the same in almost all the simulations, the value of H is changed mainly by modifying the height of the mountain.

The BOLAM3 model has been tested and compared with many other mesoscale or limited area models in the course of the COMPARE WMO project. In particular, the model evaluation conducted in "Exercise 2" of COMPARE (Georgelin et al., 2000) is relevant for the present study, because in this case the test was conducted on a well documented case of atmospheric flow over orography (PYREX project), in the presence of lee waves and wakes. BOLAM performed better than the average in reproducing various features of the flow over the orography, including lee waves and vortices, at resolutions comparable with the one employed here.

However, before using confidently our model in 3-D simulations, some specific preliminary tests have been done. First, the adequacy of the resolution employed has been checked with respect to the mountain scale, by repeating some of the dry and moist experiments at higher resolution (10 km). It turns out that the differences remain very small if compared to the typical flow perturbations we are interested to model. Second, the effect of internal model dissipation has been considered, by changing diffusion coefficients in a range of one order of magnitude around the typical values used in the experiments. Also in this case, the characteristics of the equilibrium solutions are only slightly modified and the evolution times are affected only to a small extent. Third, it has been verified that mass and energy integrals remain constant.

Once the internal model parameters have been tested, an intercomparison with results available in the literature has been attempted. At first, we have considered simulations over small amplitude obstacles ($H = 0.1$). A good agreement in the intensity of the upstream minimum and the downstream maximum of u-wind component can be observed in comparison with the analytical solution calculated by Smith (1980) and numerical solutions obtained by Smith and Grønås (1993) and Bauer (1997), using respectively the HIRLAM and RAMS models (Table 1). BOLAM3 preserves better the fore-after symmetry in the amplitude of the perturbation of the velocity component in the along-channel direction, even if, as for the other models, such values are, in absolute value, larger than the analytical ones.

Another comparison has been made with other models results, but for a weakly non-linear regime. Also in this case, solutions are very similar: the values of the three extremes of u-wind component,

Table 1. *Comparative table of the extreme values of the u-component of velocity and corresponding perturbations (ms^{-1}) obtained analytically and with different models, as regards a small amplitude obstacle ($H = 0.1$)*

	Analytical (Smith, 80)	BOLAM3	Smith–Grønås	Bauer (RAMS)
Upstream min	9.62	9.55	9.54	9.57
	−0.38	−0.45	−0.46	−0.43
Downstream max	10.38	10.45	10.44	10.48
	+0.38	+0.45	+0.44	+0.48

typical of gravity waves, are close to each other (Table 2). The drag, normalised with the analytical value, for this height is equal in our case to 1.14 and is close to the value given by the other two models (1.11).

3. Dry and moist simulations

Since our main objective is a better understanding of the dynamics of orographic precipitation, we are mainly interested in studying regions located upstream and immediately downstream of the obstacle (see also Smolarkiewicz and Rotunno, 1990).

In this section, moist solutions, as a function of different flow regimes, are compared with the respective dry cases. Moist solutions described in this section are obtained in an atmosphere where the content of relative humidity is prescribed upstream to 98%, constant up to the tropopause. For simulations with the same vertical profiles of wind, static stability and relative humidity, temperature can effectively modify solutions if condensation takes place, since it controls the absolute humidity and then the amount of latent heat that can be released. Therefore, in the experiments described below, the same upstream temperature profile has been prescribed.

3.1. Linear and quasi-linear regimes

For very low mountains ($H \leqslant 0.1$), moist solutions show the same structure of dry gravity waves, since, in this case, the air flows completely over the mountain in both dry and moist situations, and the extension of cloudy areas is very limited.

By increasing H to about 0.5 (not shown), the intensity of wind perturbations becomes larger, but the presence of humidity changes the position of speed extremes with respect to the dry case: the downstream maximum is not found near the ground anymore, but is displaced over and immediately out of the upstream saturated region above the obstacle. The upstream minimum, still near the ground, is found just upwind of the saturated area. Moreover, the intensity of perturbations becomes larger in the dry case than in the moist one, as a consequence of the fact that, in atmospheres with upstream constant N and U, horizontal wind speed perturbations are proportional to N (Durran and Klemp, 1983). However, N is not reduced everywhere, but only in saturated regions, and this makes the interpretation of results not so straightforward. The effect of latent heat reduces the perturbations of temperature as well, especially upstream and at the lowest levels. In agreement with observations (Houze, 1993), a cloud appears upstream; another cloud, placed

Table 2. *Comparative table of the extreme values of the u-component of velocity (ms^{-1}) obtained with different models, in a weakly non-linear regime ($H = 0.5$)*

	BOLAM3	Smith-Grønås	Bauer (RAMS)
Upstream min ($H = 0.5$)	7.8	7.8	7.7
Downstream max ($H = 0.5$)	12.8	13.0	12.9
Downstream min ($H = 0.5$)	8.0	7.6	7.5

downstream, may be amplified in our case by the high upper level amount of humidity used in the simulations.

A further increase in H up to 1.0 emphasises the differences between the dry and moist cases. The comparison of Fig. 1 and Fig. 2 shows that a larger amount of air flows over the obstacle in the moist case, because of the larger upstream blocking in the dry case. In fact, the contour corresponding to the ambient wind speed (10 m/s) is shifted upstream in Fig. 2 with respect to Fig. 1, so that the flow at every point at the lowest sigma level across a line through the crest parallel to the y-axis is everywhere stronger in the moist case than in the dry case. Fig. 3 shows that, in the dry situation, the stronger non-linearity of the obstacle raises the slope of the streamlines, but no wave breaking is yet observed. A secondary downstream

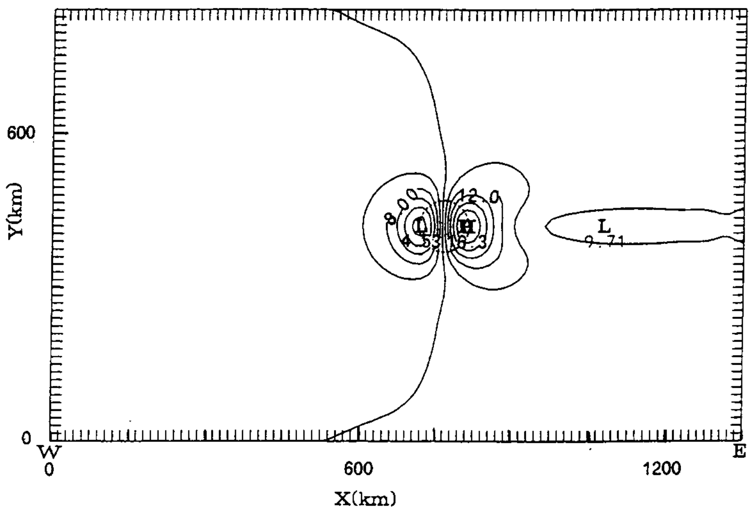

Fig. 1. $H = 1.0$, dry case: U at the lowest sigma surface after 20 h. Contour interval is 1 m/s. Only a portion of the actual domain is shown: the extreme 120 km in the northern, western, southern parts of the channel, and the eastern one third of the channel are omitted in the figure.

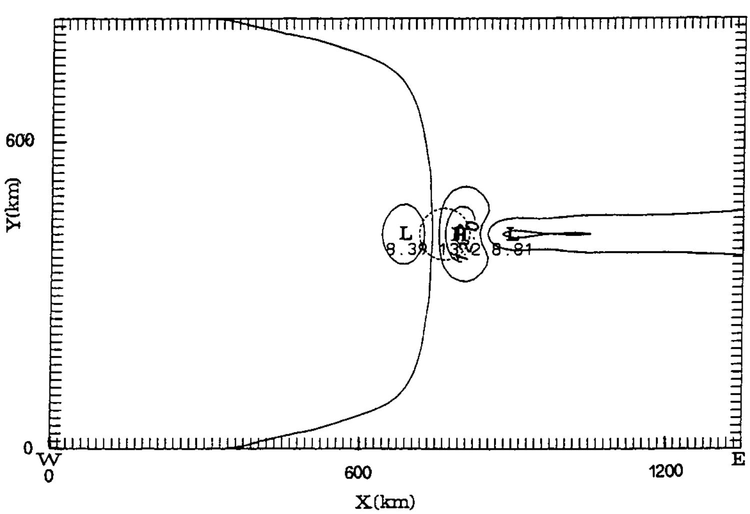

Fig. 2. As Fig. 1, but for the moist case (rh = 98%).

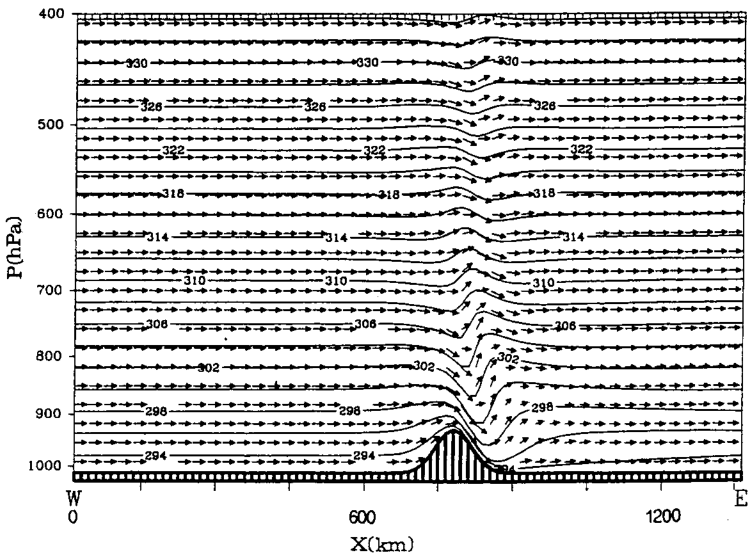

Fig. 3. $H = 1.0$, dry case: vertical cross-section of θ_e $(=\theta)$ and wind velocity along the central axis of the channel. Contour interval of θ_e is 2 K. The longitudinal extension of the domain is the same as Fig. 1. The upper part of the domain is not shown.

speed minimum is related to the extension to the ground of the upper minimum.

The moist solution is not very sensitive to the specific value of H: the flow regime does not change in a range of values around $H = 1.0$ (Fig. 4). The differences between the dry and moist cases are mainly due to the extension of the cloudy areas, as shown in Fig. 5.

H, that depends on the dry value of N, is no more the only parameter that controls the flow in the moist case, since the flow regime in the wide condensed regions is dominated by the local value of the moist Brunt–Väisäla frequency N_m (Lalas and Einaudi, 1974; Durran and Klemp, 1982b). We consider here the expression for N_m, that was proposed by Durran and Klemp (1982b) as a very good approximation to the exact form:

$$N_m^2 = g\frac{1 + (Lq_s/RT)}{1 + (\varepsilon L^2 q_s/c_p RT^2)}\left(\frac{\mathrm{d}\ln\theta}{\mathrm{d}z} + L/c_p T\frac{\mathrm{d}q_s}{\mathrm{d}z}\right) - g\frac{\mathrm{d}q_w}{\mathrm{d}z}, \quad (5)$$

where g is the gravitational acceleration, L the latent heat of vaporisation, T the absolute temperature, q_s the saturation mixing ratio, q_w the total water mixing ratio (sum of q_s and of the liquid water mixing ratio), R the dry air gas constant, ε the rate between R and the gas constant for moist air, c_p the heat capacity of dry air.

Fig. 6 shows N_m on a vertical cross-section through the central axis of the channel. Two regions of minimum, but positive, N_m appear near the mountain. The first one is located immediately upstream and over the top of the obstacle and corresponds to a region of condensation. The situation is completely different from the dry case (Fig. 7), in which a region of higher stability is observed in the region above the mountain, due to the shrinking of the isentropic surfaces. The second region of low stability in the moist case is located immediately downstream, and can be separated into two different sub-regions: one is due to condensation in the downstream cloud, the other is related to the steepening of the isentropes in the descent of dry air from the top of the mountain.

Since the horizontal wavelength is unchanged and the vertical one, inversely proportional to N, is reduced, the pattern results steeper than in the dry case, and the phase shift is diminished, as observed in 2-D simulations (Jusem and Barcilon, 1985).

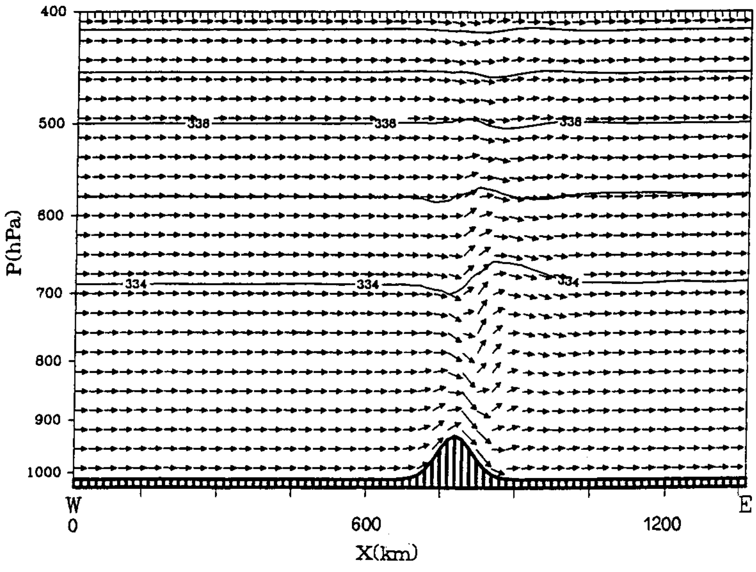

Fig. 4. As Fig. 3, but for the moist case.

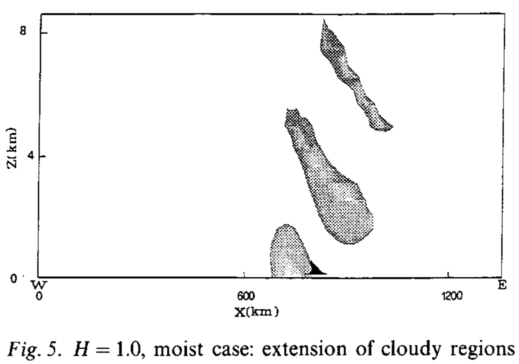

Fig. 5. $H = 1.0$, moist case: extension of cloudy regions along the central axis of the channel after 28 h. The low level orographic cloud partially masks the mountain (visible as a dark "tail" on the right side of the cloud). The eastern one third and the upper part of the domain are not shown.

3.2. *Non-linear regimes: wave breaking and flow splitting*

The most significant differences among dry and moist simulations occur for the set of parameters where non-linear effects, such as wave breaking or flow splitting, become important in modifying the flow regime. It is interesting, therefore, to analyse what happens in such simulations and how the appearance of stagnation points (Smith, 1989b) can be influenced by the presence of humidity.

The differences between dry and moist cases for $H = 1.25$ become striking (not shown). In the dry simulations, where zonal flow reversal occurs downstream after about one day of integration, a couple of vortices aloft can be distinguished downstream (the symmetry in the transversal direction is generally imposed by the symmetric conditions in the model and in the initial conditions). No upstream flow reversal can be observed, and the influence of wave breaking and downstream phenomena on upstream conditions is small in comparison with 2-D simulations (Pierrehumbert and Wyman, 1985). The downstream reversed flow reaches its maximum intensity immediately after the breaking, when the drag has a strong decrease (see also Section 4). Warm vortices, that move towards the ground but do not reach it yet, are progressively weakened and advected downstream. The presence of the reversal limits the maximum value that the u-wind component can reach downstream, preventing a strong descent of air along the central axis: therefore the maximum u-component is observed before the overturning of isentropes occurs.

The moist solution, unlike the dry one, does not show overturning of isentropes for $H = 1.25$

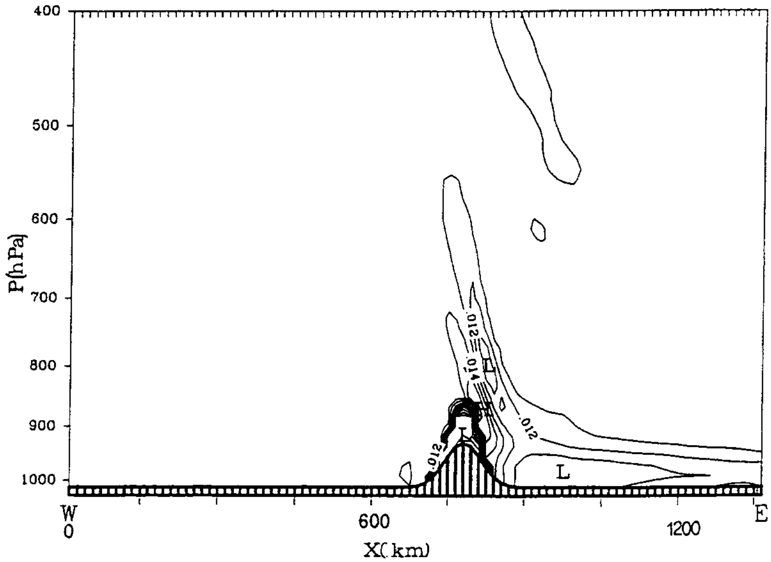

Fig. 6. $H = 1.0$, moist case: vertical cross-section of effective Brunt–Väisala frequency (see text) N_m along the central axis of the channel after 20 h. Contour interval is $1 \times 10^{-3}\ s^{-1}$. A positive minimum of $+0.004\ s^{-1}$ is present above the mountain.

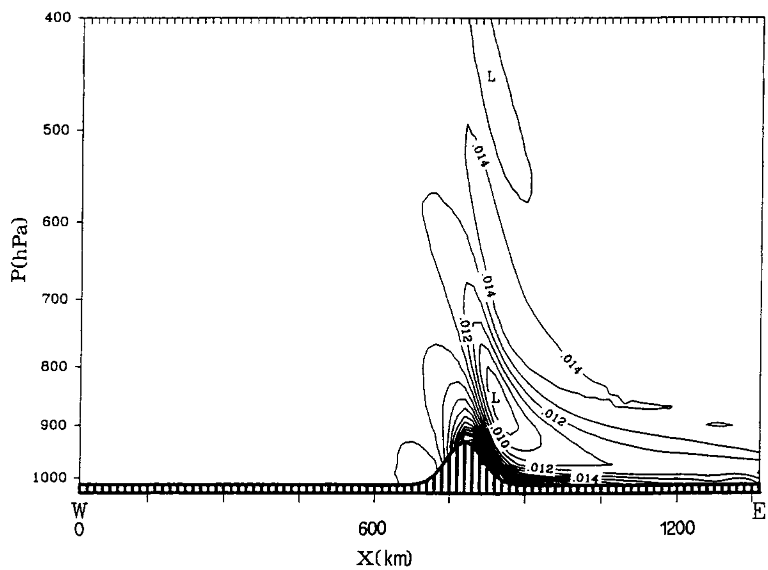

Fig. 7. As Fig. 6, but for the dry case. A maximum of N is present immediately above the mountain.

(not shown). No significant qualitative difference can be observed in this case with respect to $H =$ 1.0, apart from proportionally larger perturbations and vertical motions. In comparison with the dry case, the maximum u-component is still located along the central axis of the channel.

In the dry case, for higher mountains ($H = 1.5$), the breaking appears in the simulation after a smaller period of time (about 12 h). An upstream blocked region, although confined to a narrow area, occurs at the same time of wave breaking and remains stationary during the whole simulation.

Fig. 8 shows that the region of flow reversal has reached the surface and is associated with a pair of lee vortices. The presence of the vortices obstructs the downslope airflow and a larger amount of air is forced to flow around. Two regions of diffluence can be distinguished near the top, due to the motion around the vortices, one immediately upstream and the other downstream.

Additional simulations have been made still with free slip conditions at the surface, but including internal dissipation aimed at parameterising turbulence for low or negative values of the Richardson number. In fact, gravity wave breaking is associated with local negative static stability and wind shear that may induce important turbulent dissipation. We have generally neglected this aspect in the course of our study, since our aim was mainly to tackle the basic inviscid problem (except for the numerical internal diffusion), but an assessment of the importance of the internal diffusion in the presence of GWB is relevant. Some differences with respect to the previous experiments can actually be observed in the simulations with turbulent closure after the breaking occurs. In particular, the region of downstream reversal remains confined at mid levels, where it occurs initially, and it does not move closer to the ground, in contrast with the inviscid case. Furthermore, the intensity of the associated minimum wind speed remains almost constant after the overturning, so that a stationary final value appears earlier than in the inviscid case. These results could explain the discrepancies in time evolution of the downstream patterns that have been observed in literature among simulations of orographic flows (see Crook et al., 1990; Smith and Grønås, 1993; Rotunno and Smolarkiewicz, 1991). However, the impact of internal dissipation on the flow upstream and above the obstacle, which we are mainly interested in here, turns out to be small. Therefore, we think that it may be considered not so relevant for the purposes considered in the present study.

Fig. 9 shows that a wave breaking, even if weaker, can be observed for $H = 1.5$ also in the moist case: it appears, however, later than in the dry case and the overturning modifies strongly the flow features. It can be noticed in Fig. 10 that the reversed flow cannot reach the ground, as in the dry case with a smaller mountain height ($H = 1.25$). The position of the downstream u-wind component maximum moves laterally and is displaced far downstream.

The extension of the area with precipitation and that of the condensed region increases with H.

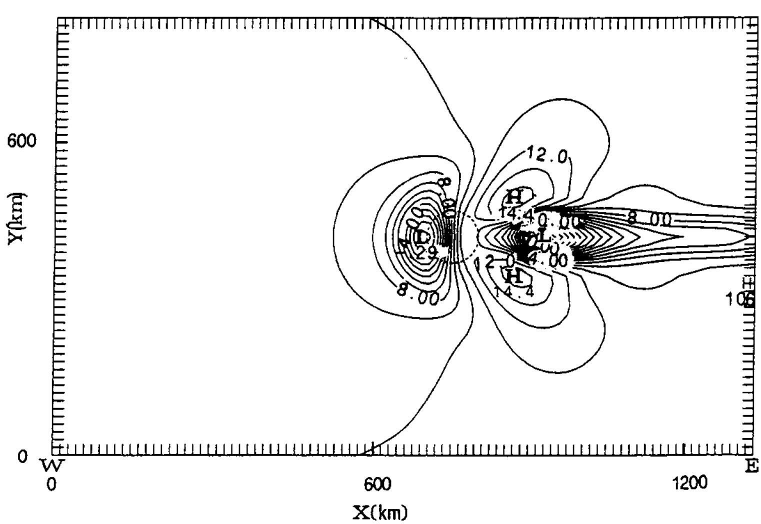

Fig. 8. As Fig. 1 (dry case), but for $H = 1.5$.

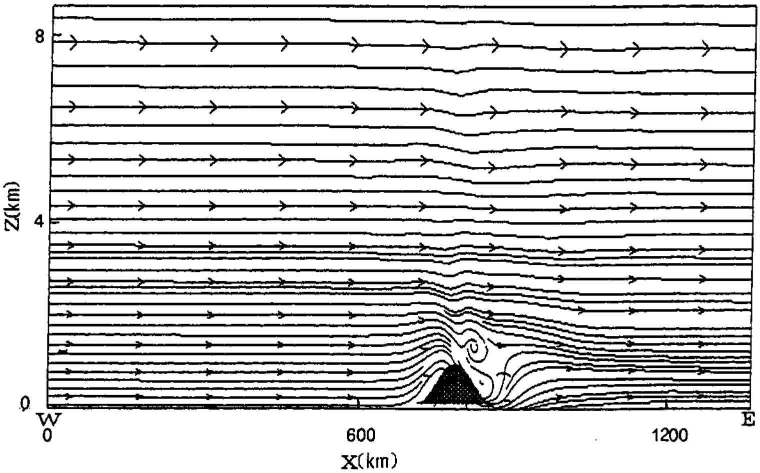

Fig. 9. $H = 1.5$, moist case: streamlines along the central axis of the channel after 32 h. The overturning of the streamlines is apparent immediately downstream the obstacle. The eastern one third and the upper part of the channel are not shown.

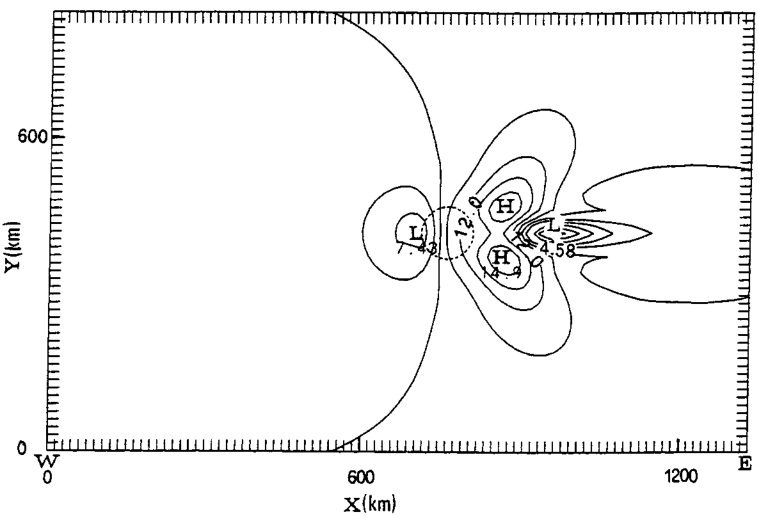

Fig. 10. As Fig. 1, but for the moist case after 40 h, with $H = 1.5$.

The volume of clouds, especially of those that, for $H = 1.5$, can be distinguished downstream (Fig. 11), fluctuates in time.

For larger values of H ($H = 2.0$, not shown), wave breaking and lee vortices at the ground appear immediately after the beginning of the simulation in the dry case, while two different breakings, the first appearing only 12 h after the beginning, can be observed in the moist case. It is interesting to notice that the values of the u-wind component extremes and those of the drag change weakly in time, as in Schär and Durran's simulations (Schär and Durran, 1997): Fig. 12 shows that these values are comprised in a range of at

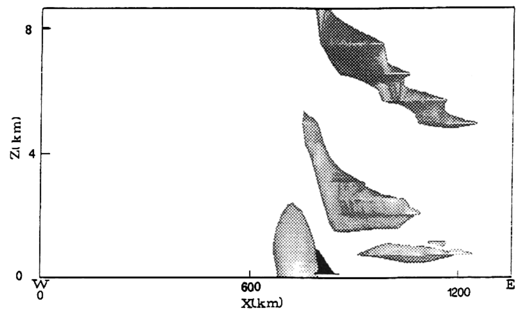

Fig. 11. As Fig. 5, but for $H = 1.5$.

most 20% around the average values. The oscillation of the intensity of the drag, exhibited for this value of H by some other models (Miranda and James, 1992), has not been observed in our simulation.

3.3. *High mountains*

For much higher values of the adimensional mountain height ($H > 2$), significant differences can be seen in comparison with the previous cases. Fig. 13 shows the zonal (along channel) wind perturbation for the dry case with $H = 5.0$. In dry simulations, the circulation is completely around the obstacle up to a few hundred meters below the top of the mountain, apart from the layer near the bottom, where a weak descending motion is present upstream. For several aspects, and especially for the general weakness of the vertical component of motion at low and intermediate levels near the mountain, if compared with deviation of the horizontal motion induced by the obstacle, such a solution is similar to the limiting case of a two-dimensional potential flow, for which Drazin (1961) presented an analytical solution. This solution has been considered more recently by Smolarkiewicz and Rotunno (1989) and Hunt et al. (1997), to (partly) explain the flow regime around high obstacles. Only near the mountain top, ascending vertical motions can be observed. A significant departure from the theory is due to the presence of wide vortices with vertical axis, extending in the lee of the mountain from the ground up to about 2000 m, and moving progressively downstream. Apart from this aspect, the solution can be considered almost stationary. There is no upstream reversed flow, but all the air particles next to the obstacle are almost stagnant.

The moist solution (Fig. 14) differs slightly from the dry one, although the upstream strong deceleration is confined closer to the obstacle. Also the

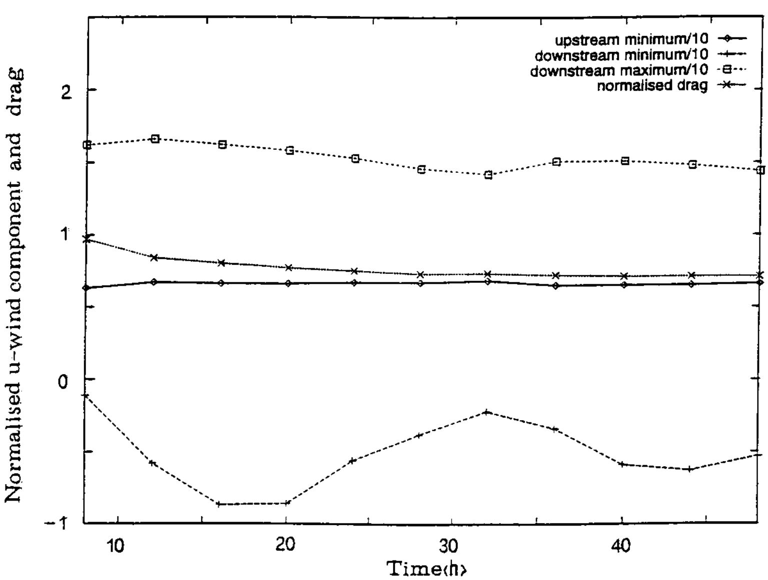

Fig. 12. $H = 2.0$, dry case: time variation of the intensity of the extremes of the u-wind component, normalised with the velocity at the entrance of the channel (10 m/s), and of the normalised drag.

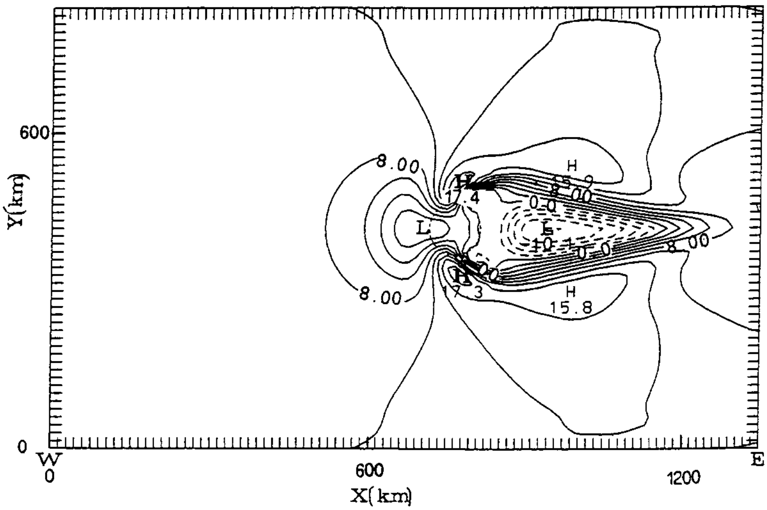

Fig. 13. As Fig. 1 (dry case), but for $H = 5.0$, after 32 h. Contour interval is 2 m/s.

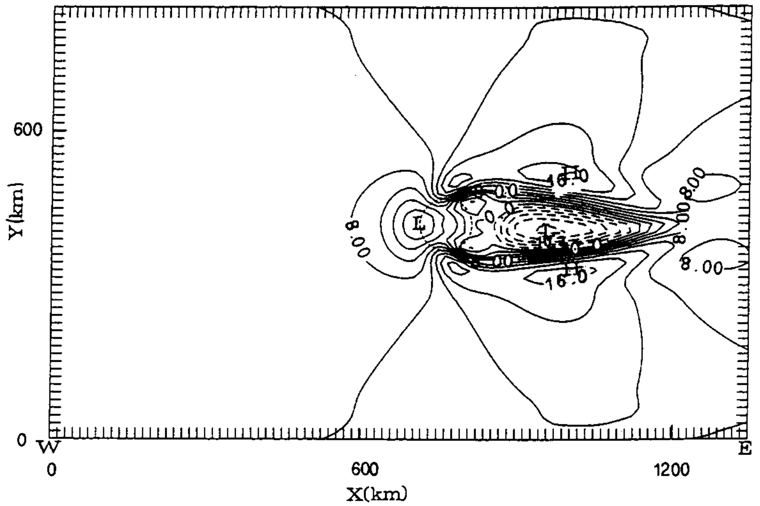

Fig. 14. As Fig. 13, but for the moist case.

intensity of the extremes of u-wind component and of the drag are very similar. The main difference is related to the amount of "flow over", that is larger: a stronger descent of air can be observed at both sides of the obstacle, where the maximum u-component can be observed. It appears, in fact, that the cross mountain wind just above the top of the mountain in the dry case is about 3 m/s, whereas it is about 4 m/s in the moist case.

The intensity of precipitation is reduced with respect to the case of lower H, but the extension of the involved area and the magnitude of the integral of precipitation are larger.

Additional simulations have been made for $H = 10$. Since, by further increasing of the height of the mountain, the slope would become unrealistic for the Earth and too large to be represented correctly in the model, the new value of H has been obtained by halving the velocity at the entrance of the channel. The upstream vortices in this case are extremely reduced, and the solution agrees well with Smolarkiewicz and Rotunno

(1989) numerical results and with the analytical potential flow solution. A strong confluence, observed immediately downstream of the obstacle in place of the diffluence due to the presence of lee vortices, is associated with a strong ascending motion and a deep cloud there, while the upstream condensation is strongly reduced for this adimensional height.

4. Additional results and discussion

In the attempt of completing and better quantifying in a systematic way the results obtained in the previous section, further simulations with obstacles of different heights have been analysed. Moreover, numerical experiments with different values of relative humidity have been performed, in order to study the dependence of solutions on this field. As we will show, results are very sensitive to both parameters. Parameters used in our simulations form a combination of all the values of relative humidity and height shown in Table 3.

The general results derived from the series of systematic moist simulations, in comparison also with the corresponding dry cases, are summarised below.

• A stronger component of "flow over" is generally observed in the moist cases. Therefore, the intensity of perturbations of the u-wind component is reduced as humidity increases. Moreover, the differences with dry cases are larger for heights next to the critical value for dry wave breaking, while are reduced for both very small and very high obstacles.

• The extension of condensed regions increases with H, and the upstream cloud moves progressively further upstream.

• Since condensation weakens the amplitude of gravity waves, we expect a shift in the overturning of streamlines to higher mountain heights. In fact, wave breaking, observed in dry simulations with $H \sim 1.2$, does not appear in moist cases for the same height: while for $H = 1.25$ it is still present for rh $\leqslant 95\%$, it is not observed for higher values of humidity. The difference is more striking for $H = 1.50$: the lee wave breaks for any humidity value, apart from the case rh $= 100\%$, but two different regions of overturning can be seen for rh $\leqslant 95\%$, in the course of our simulations. Only in the dry case the vortices reach the ground, generating two lee warm reversed circulations. For $H = 2.0$, breaking is observed already at the beginning of the simulation and for rh $\leqslant 95\%$. No overturning can be seen for rh $= 100\%$. For intermediate values of humidity, also in this case two temporally distinct breaking episodes occur in the simulations. For rh $= 100\%$, the critical height for breaking is $H \sim 2.5$. For higher mountains and for any value of relative humidity, horizontal flow splitting reduces the mountain lifting effect and gravity waves intensity, preventing the generation of further wave breaking.

• An effect of the overturning of the isentropes is the decreasing of the downstream u-component maximum occurring immediately after the breaking, in both situations. Therefore, as already observed by Bauer (1997), the effects are opposite to what occurs in 2-D experiments. Fig. 15 shows the values of the maximum of u-wind component, observed after the breaking, as a function of H. A reduction can be observed for heights slightly larger than the critical value required for breaking. Then, when the lateral flow is stronger, the max-

Table 3. *Table with all the values of relative humidity and adimensional mountain height used in simulations*

H	0.1	0.5	1.0	1.25	1.5	2.0	3.0	4.0	5.0
R.H.		1	80	85	90	95	98	100	

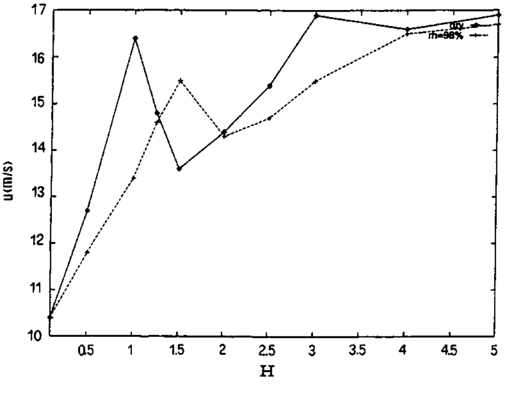

Fig. 15. Intensity of downstream u-wind component maximum versus H for the dry and moist cases. For values of H corresponding to breaking, the intensity is observed after wave breaking.

imum tends to increase again at both sides of the central axis. For very high obstacles, in conditions of prevalent "flow around", the intensity of the downstream maximum does not appear to be sensitive either to H or to relative humidity.

- As in most of the observed events, the maximum intensity of precipitation increases with H, except for very high mountains. The ability of moist air near the ground to flow over an obstacle strongly controls the orographic precipitation. Smith (1989a) studied the case of flow over the Hawaii islands, a group of isolated mountains of different height and geometry, but exposed to the same flow, applying his regime diagram for the individuation of wave breaking and flow splitting. The highest and narrow mountains, where the depth of the air mass lifted over the obstacle is small, receive less precipitation, as a consequence of the larger lateral deflection and of the fact that only the dry air near the top can flow over. In our simulations, precipitation is observed only upstream, apart from very low mountains. The affected area, together with the upstream cloud, moves progressively upstream at increasing height. Fig. 16 shows precipitation versus H for the two cases of highest relative humidity: the values shown in the figure have been obtained immediately after the transient phase and remain almost constant. The intensity increases up to $H = 3.0$, remains almost constant between $H = 3.0$ and 4.0, and decreases for higher values, when "flow around" is stronger.

It should be noticed that, for a fixed height, a more pronounced lateral deflection appears with decreasing humidity, and so the critical height for "flow around" is lower in a drier atmosphere. This explains, to some extent, why the maximum intensity of precipitation (and also of integrated precipitation) is observed for larger H, for increasing values of relative humidity ($H = 2.0$ for rh = 90%, $H = 3.0$ for rh = 95%–98%, $H = 4.0$ for rh = 100%), as shown in Fig. 17.

The maximum intensity of precipitation that our model produces (about 65 mm/day) is weak in comparison with the observed values in flood producing events. So, heavy rain situations need a combination of orography and of some meteorological perturbations, such as frontal or convective systems (see, for example, Smith, 1982; Buzzi and Foschini, 2000).

- The upstream minimum, the only u-wind component extreme that reaches rapidly a stationary state for any value of height of the obstacle, is shown as a function of H in Fig. 18. An upstream reversal can be seen in dry simulations already for $H \sim 1.5$. This corresponds to a descending current, confined upstream of the obstacle at low levels, that forms a separated region of clockwise circulation in a vertical plane. As H increases above 2.0, this reversal flow decreases, corresponding to a transition towards a more potential "flow around" solution (Drazin, 1961; Hunt et al., 1997). In moist cases, the intensity of the (still positive) upstream minimum decreases with increasing relative

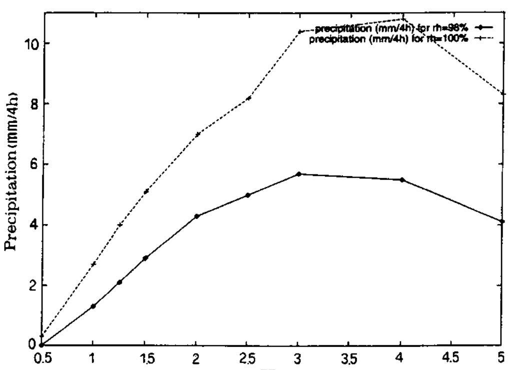

Fig. 16. Maximum of upstream precipitation, accumulated over 4 h, versus H, in simulations with two different values of humidity (rh = 98% and 100%). The values are observed immediately after the transient phase; later, they remain almost constant during the simulations.

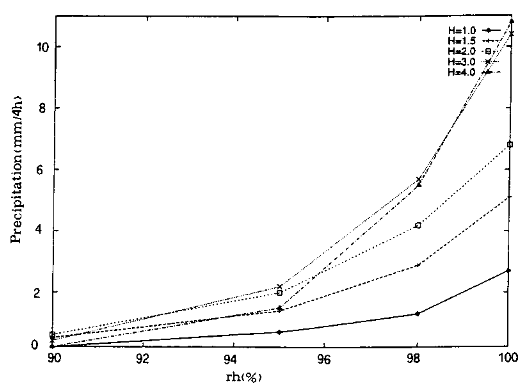

Fig. 17. Maximum intensity of precipitation (4 h integrated) versus relative humidity (rh), for different values of H. The values, observed after the initial transient phase, remain almost costant during the simulations.

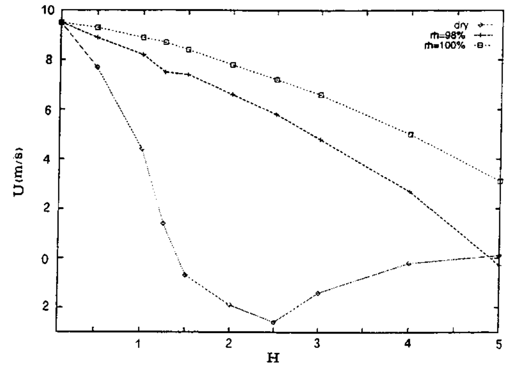

Fig. 18. Intensity of upstream u-wind component minimum versus H, for dry and moist simulations with two different values of humidity (rh = 98% and 100%). For any value of the height of the obstacle, wind speed rapidly reaches a value that remains almost constant during the simulation.

humidity for all the values of H. However, as Fig. 19 shows, for $H = 4.0$ and for rh = 95%, a stronger reversed flow than in the dry case is observed. The presence of humidity moves the formation of a reversed flow to higher values of H, or suppresses it in the most humid cases (see again Fig. 19). In fact, the nearly potential flow solution is realised, with condensation, only for very high mountains. Differences among the completely dry and the rh = 90% cases are significant only for $H = 1.5$, when the upstream reversal occurs in dry simulations.

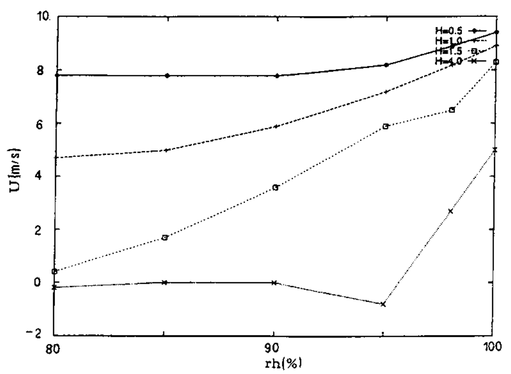

Fig. 19. Intensity of upstream u-wind component minimum versus relative humidity (rh), for several values of H. For any value of the height of the obstacle, wind speed rapidly reaches a value that remains almost constant during the simulations.

• The determination of the dependence of the intensity of the drag on different flow parameters is a problem of general interest. Understanding the non-linear behaviour of the drag is important for parameterizing mountain drag in global models. Observations and numerical experiments have shown that, in a non-linear regime, the drag can be one order of magnitude stronger than in linear theory (Bacmeister and Pierrehumbert, 1988). The presence of humidity and of the consequent upstream condensation and downstream evaporation reduce the amplitudes of pressure perturbations, and so the intensity of the drag. Our results show that, especially for low mountains, a change of only 2% in relative humidity, for values near saturation, can strongly modify the drag. The values shown in Fig. 20 and Fig. 21 are the quasi-stationary results after the last observed breaking. Fig. 20 shows that the intensity of the drag versus H has a similar behaviour in dry and moist cases: it increases up to the critical height for breaking, and then decreases for higher H, finally reaching an asymptotic value for high obstacles. However, for rh = 98% the drag decreases from $H = 0.1$ to $H = 0.5$: for such very small heights, the extension of saturated areas is strongly reduced, and the flow is very similar to the dry case.

For H between 0.5 and 1.0, the drag remains almost constant, while increases only for higher values of H. It has been verified that the intensity of the drag, for $H \geqslant 2.0$, is very similar in moist

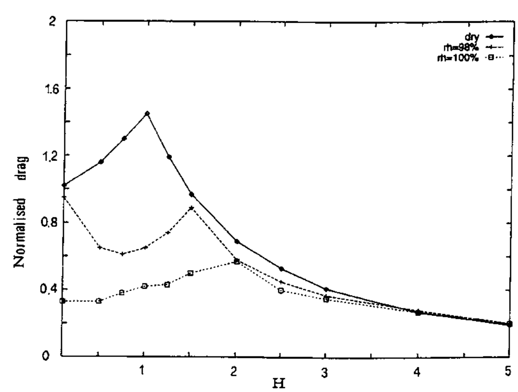

Fig. 20. Intensity of normalised drag versus H, for dry and moist simulations with two different values of humidity (rh = 98% and 100%). The values of drag are observed after wave breaking.

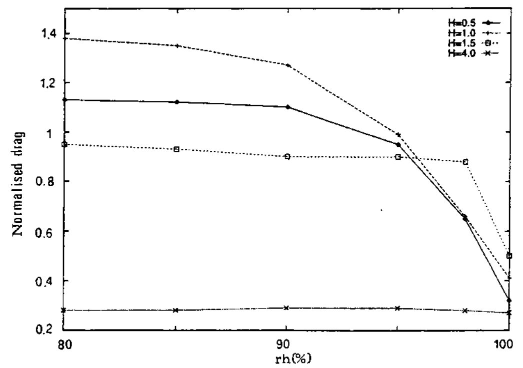

Fig. 21. Intensity of normalised drag versus relative humidity (rh), for different values of H. The values in the figure are observed after wave breaking.

and dry simulations, confirming that differences in the flow regime are reduced for high mountains (Fig. 20 and Fig. 21). Note that in the case $H = 1.5$ the drag is independent of rh for value of rh $\leqslant 98\%$, but drops substantially for rh $= 100\%$. Significant differences between the dry case and the case with rh $= 90\%$ are observed only for $H \approx 1.5$.

5. Conclusions

Numerical simulations have been made with a mesoscale model, in order to study the problem of a moist stratified flow over an idealised three-dimensional topography, also by comparing the humid cases with the corresponding dry cases. Simulations have been carried out with several different values of atmospheric humidity and adimensional height of the mountain H. Results appear to be very sensitive to both parameters.

First of all, we have shown, whenever appropriate, that our results are mainly consistent with previous studies of dry flow over orography. This is true in the dry reference cases, but also in cases where the flow modifications due to the effects of humidity are minor, either because the humidity itself is small in the basic state or because the flow regime is well defined and qualitatively similar to that of the corresponding dry cases. This turns out to be the case for very small and large values of adimensional mountain height. In the most critical case of intermediate flow regimes, humidity introduces changes in the flow that are not easily interpreted, mainly due to the non-uniformity of latent heat release processes. However, such changes can be, to some extent, interpreted in terms of changes in the field of effective (moist) static stability N_m, depending on the moisture distribution and on the occurrence of condensation. In fact, the values of the Brunt–Väisala frequency are very different in dry and saturated regions. However, the interpretation of the simulations is not so straightforward: the presence of saturated regions depends on the flow itself, and especially on the vertical motion field which, near the obstacle, can vary widely as a function of the flow regime. The "local" interpretation of flow modifications in terms of modified static stability seems to be more appropriate in the near upstream and over the obstacle, where the vertical velocity is mainly upward, than further downstream and far above the obstacle, where the vertical velocity fluctuates in a more complex way.

In general, the experiments indicate that the presence of humidity in the atmosphere can effectively change the flow type with respect to the dry case, for the same upstream wind and temperature profiles, especially for values of H in the range for which changes of flow regime occur, depending also on how close the atmosphere is to saturation. In fact, if saturation does not occur, either because humidity is too low or because vertical displacements are too small, the effects of humidity become negligible. If, on the opposite, the upstream relative humidity is close to 100%, even weak ascending motions can easily bring to saturation. In this case, the differences between the moist and humid cases are large, especially for intermediate values of obstacle height and if the absolute humidity is not too small (i.e., if temperature is sufficiently high) to allow for significant latent heat release. In particular, the differences observed for heights next to the critical value for the occurrence of dry wave breaking are dramatic also for relative humidity equal to 90% (with a surface temperature around 20°C). For this value of humidity and for lower and higher heights of the mountain, significant differences with the dry cases are not observed. The comparison of dry and moist simulations with rh $= 98\%$ and $H = 1.50$ shows that in the moist case, unlike in the dry one, the region of flow reversal does not reach the ground and the maximum intensity of the wind is still observed at the ground along the central axis. Furthermore, no lee vortices can be seen in this case, since in our simulations they appear to be a consequence of the downward motion of the reversed region.

Differences between dry and moist cases become less evident for very high mountains, since in this case the flow is less sensitive to static stability (unless the stratification becomes neutral or unstable).

The changes produced in the orographic flow are due to the release of latent heat that favours the "flow over" regime by decreasing the effective static stability of the ascending saturated flow. This effect has important consequences on the distribution and the amount of precipitation. The maximum intensity of precipitation increases with H up to a threshold height, that is lower for a drier atmosphere. For mountains higher than this threshold, the amount of air deflected around increases and precipitation is reduced.

The occurrence of wave breaking is moved by condensation to higher mountain heights, more strongly for moister atmospheres, since humidity tends to decrease the wave amplitude: so, the critical height grows for increasing relative humidity.

Some interesting effects of the overturning of the isentropes, that appear also in dry simulations, are the reduction of the downstream u-wind component maximum and of the intensity of the drag immediately after the breaking has established. Other non-linear effects such as, for example, the formation of upstream stagnation regions or of lee vortices, are generally confined to larger values of mountain heights than in the dry case, or are completely suppressed.

The drag exerted by topography on the flow is lower if compared with the dry case: the release of latent heat reduces the intensity of the pressure perturbations induced by adiabatic motions, and hence the drag. Generally, the intensity of the drag versus H shows the same behaviour in dry and moist cases: it increases up to the height of first appearance of wave breaking and then decreases, reaching the same asymptotic value in dry and moist simulations for very high H. However, a strong decrease in the range from very small heights to values of $H \approx 0.5$ can be observed, but only in the $\mathrm{rh} = 98\%$ case. These results may be relevant for the parameterisations of momentum flux over mountainous regions in global models, even though the inclusion of viscous drag may limit the importance of these results for the realistic atmospheric states.

6. Acknowledgements

This work has been partially supported by the European Social Fund (ESF) and by the EU project HERA (ENV4-CT96-0332). We are indebted to one referee for constructive suggestions.

REFERENCES

Bacmeister, J. T. and Pierrehumbert, R. T. 1988. On high-drag states of nonlinear stratified flow over an obstacle. *J. Atmos. Sci.* **45**, 63–80.

Baines, P. G. and Hoinka, K. P. 1985. Stratified flow over two-dimensional topography in fluid of infinite depth: a laboratory simulation. *J. Atmos. Sci.* **42**, 1614–1630.

Barcilon, A. and Fitzjarrald, J. 1985. A non linear steady model for moist hydrostatic mountain waves. *J. Atmos. Sci.* **42**, 58–67.

Barcilon, A., Jusem, J. C. and Drazin, P. G. 1979. On the two-dimensional hydrostatic flow of a stream of moist air over a mountain ridge. *Geophys. Astrophys. Fluid Dyn.* **13**, 125–140.

Bauer, M. H. 1997. *Three-dimensional numerical simulations of the influence of the horizontal aspect ratio on flow over and around a mesoscale mountain.* PhD thesis, University of Innsbruck, Austria.

Buzzi, A. and Malguzzi, P. 1997. The Bolam III model: recent improvements and results. *MAP Newsletters* **7**, 98–99.

Buzzi, A. and Foschini, L. 1998. Numerical experiments on the dynamical effects of latent heat exchanges and topographic forcing in MAP case studies. *MAP Newsletters* **9**, 26–27.

Buzzi, A. and Foschini, L. 2000. Mesoscale meteorological features associated with heavy precipitation in the Southern Alpine Region. *Meteorol. Atmos. Phys.* **72**, 131–146.

Buzzi, A., Fantini, M., Malguzzi, P. and Nerozzi, P. 1994. Validation of a limited area model in cases of Mediterranean cyclogenesis: surface fields and precipitation scores. *Meteorol. Atmos. Phys.* **53**, 137–153.

Buzzi, A., Foschini, L. and Malguzzi, P. 1998a. The Piedmont flood of 1994: an analysis of the concurrent meteorological processes based on systematic numerical experimentation. *Proceedings of the 25th International Conference on Alpine meteorology*, Torino, Italy, 14–19 September, Regione Piemonte, 8–12.

Buzzi, A., Tartaglione, N. and Malguzzi, P. 1998b. Numerical simulations of the 1994 Piedmont flood: role of orography and moist processes. *Mon. Wea. Rev.* **126**, 2369–2383.

Cotton, W. R. and Anthes, R. A. 1989. *Storm and cloud dynamics*. Academic Press, New York, 883 pp.

Crook, N. A., Clark, T. L. and Moncrieff, M. W. 1990. The Denver cyclone. Part I: Generation in low Froude number flow. *J. Atmos. Sci.* **47**, 2725–2742.

Davies, H. C. 1976. A lateral boundary formulation for multilevel prediction models. *Q. J. Roy. Meteor. Soc.* **102**, 405–418.

Drazin, P. G. 1961. On the steady flow of a fluid of variable density past an obstacle. *Tellus* **13**, 239–251.

Durran, D. R. and Klemp, J. B. 1982a. The effects of moisture on trapped lee waves. *J. Atmos. Sci.* **39**, 2490–2506.

Durran, D. R. and Klemp, J. B. 1982b. On the effects of moisture on Brunt–Väisäla frequency. *J. Atmos. Sci.* **39**, 2152–2158.

Durran, D. R. and Klemp, J. B. 1983. A compressible model for the simulation of moist mountain waves. *Mon. Wea. Rev.* **44**, 2341–2361.

Fraser, A. B., Easter, R. C. and Hobbes, P. V. 1973. A theoretical study of the flow of air and fallout of solid precipitation over mountainous terrain. Part I: Airflow model. *J. Atmos. Sci.* **30**, 801–812.

Georgelin, M., Bougeault, P., Black, T., Brzovic, N., Buzzi, A., Calvo, J., Cass, V., Desgagné, M., El-Khatib, R., Geleyn, J. F., Holt, T., Hong, S.-Y., Kato, T., Katzfey, J., Kurihara, K., Lacroix, B., Lalaurette, F., Lemaitre, Y., Mailhot, J., Majewski, D., Malguzzi, P., Masson, V., Mcgregor, J., Minguzzi, E., Paccagnella, T. and Wilson, C. 2000. The second COMPARE exercise: a model intercomparison using a case of a typical mesoscale orographic flow, the PYREX IOP3. *Q. J. Roy. Meteor. Soc.* **126**, 991–1030.

Houze, R. A. 1993. *Cloud dynamics*. Academic Press, New York, 573 pp.

Hunt, J. C. R., Feng, Y., Linden, P. F., Greenslade, M. D. and Mobbs, S. D. 1997. Low-Froude-number stable flows past mountains. *Il Nuovo Cimento* **20**, 261–272.

Jusem, J. C. and Barcilon, A. 1985. Simulations of moist, mountain waves with an anelastic model. *Geophys. Astrophys. Fluid Dyn.* **33**, 259–276.

Katzfey, J. J. 1995. Simulations of extremes New Zealand precipitation events. Part II: Mechanism of precipitation development. *Mon. Wea. Rev.* **123**, 755–775.

Klemp, J. B. and Lilly, D. K. 1978. Numerical simulation of hydrostatic mountain waves. *J. Atmos. Sci.* **35**, 78–107.

Lalas, D. P. and Einaudi, F. 1974. On the correct use of the wet adiabatic lapse rate in stability criteria of a saturated atmosphere. *J. Appl. Meteor.* **13**, 318–324.

Lehmann, R. 1993. On the choice of relaxation coefficients for Davies' lateral boundaries scheme for regional weather prediction models. *Meteorol. Atmos. Phys.* **52**, 1–14.

Lilly, D. K. and Durran, D. R. 1983. Stably stratified moist airflow over mountainous terrain. *Proceedings of the 1st Sino-Am. Workshop on Mountain meteorology*, Reiter, E. R., Baozhen, Z. and Yongfu, Q., Eds., Science Press, Beijing, and Amer. Meteor. Soc, Boston, 569–608.

Malguzzi, P. and Tartaglione, N. 1999. An economical second order advection scheme for explicit numerical weather prediction. *Q. J. Roy. Meteor. Soc.* **125**, 2291–2303.

Miglietta, M. M. and Buzzi, A. 1999. Study of moist flow over an isolated 3D topography with a mesoscale model. *MAP Newsletter* **11**, 18–19.

Miranda, P. M. A. and James, I. N. 1992. Non-linear three-dimensional effects on gravity-wave drag: splitting flow and breaking waves. *Q. J. Roy. Meteor. Soc.* **118**, 1057–1081.

Palm, E. 1953. On the formation of surface wind over a corrugated bed and on the development of mountain waves. *Astrophysica Norvegica* **5**, 61.

Pierrehumbert, R. T. and Wyman, B. 1985. Upstream effects of mesoscale mountains. *J. Atmos. Sci.* **42**, 977–1003.

Rotunno, R. and Smolarkiewicz, P. K. 1991. Further results on lee vortices in low-Froude-number flow. *J. Atmos. Sci.* **48**, 2204–2211.

Schär, C. and Durran, D. R. 1997. Vortex formation and vortex shedding in continuously stratified flows past isolated topography. *J. Atmos. Sci.* **54**, 534–554.

Schultz, P. 1995. An explicit cloud physics parameterization for operational numerical weather prediction. *Mon. Wea. Rev.* **123**, 3331–3343.

Smith, R. B. 1979. The influence of mountains on the atmosphere. *Adv. Geophys.* **21**, 87–230.

Smith, R. B. 1980. Linear theory of stratified hydrostatic flow past an isolated mountain. *Tellus* **32**, 348–364.

Smith, R. B. 1982. A differential advection model of orographic rain. *Mon. Wea. Rev.* **110**, 306–309.

Smith, R. B. 1989a. Hydrostatic airflow over mountains. *Adv. Geophys.* **31**, 1–41.

Smith, R. B. 1989b. Mountain-induced stagnation points in hydrostatic flow. *Tellus* **41A**, 270–274.

Smith, R. B. and Grønås, S. 1993. Stagnation points and bifurcation in 3-D mountain airflow. *Tellus* **45A**, 28–43.

Smith, R. B. and Lin, Y. L. 1982. The addition of heat to a stratified airstream with application to the dynamics of orographic rain. *Q. J. Roy. Meteor. Soc.* **108**, 353–378.

Smolarkiewicz, P. K. and Rotunno, R. 1989. Low Froude number past three-dimensional obstacles. Part I: baroclinically generated lee vortices. *J. Atmos. Sci.* **46**, 1154–1164.

Smolarkiewicz, P. K. and Rotunno, R. 1990. Low Froude number past three-dimensional obstacles. Part II: upwind flow reversal zone. *J. Atmos. Sci.* **47**, 1498–1511.